Polarization and Phase-Shifting for 3D Scanning of Translucent Objects

Tongbo Chen Hendrik P. A. Lensch Christian Fuchs Hans-Peter Seidel
MPI Informatik

Abstract

Translucent objects pose a difficult problem for traditional structured light 3D scanning techniques. Subsurface scattering corrupts the range estimation in two ways: by drastically reducing the signal-to-noise ratio and by shifting the intensity peak beneath the surface to a point which does not coincide with the point of incidence. In this paper we analyze and compare two descattering methods in order to obtain reliable 3D coordinates for translucent objects. By using polarization-difference imaging, subsurface scattering can be filtered out because multiple scattering randomizes the polarization direction of light while the surface reflectance partially keeps the polarization direction of the illumination. The descattered reflectance can be used for reliable 3D reconstruction using traditional optical 3D scanning techniques, such as structured light. Phase-shifting is another effective descattering technique if the frequency of the projected pattern is sufficiently high. We demonstrate the performance of these two techniques and the combination of them on scanning real-world translucent objects.

1. Introduction

For a number of scenes, structured light 3D scanning techniques run into the problem that the signal observed by the camera for a surface point is actually not only due to direct reflection of the projected pattern but instead contains polluting signals originating from ambient illumination, interreflections from other scene parts, or from subsurface scattering. These effects are most prominent in translucent objects where the directly reflected signal is furthermore weakened since the incident light is diffused inside the material instead of being fully reflected at the surface. Subsurface scattering can of course be excluded completely if the object's surface is painted before scanning, as it is done frequently. In this paper, we propose 3D scanning techniques which are inherently robust against subsurface scattering.

In order to obtain reliable scans of translucent objects one has to separate the direct reflection from the pollution due to multiple interreflections or scattering. One approach to descattering is to use the fact that light scattered multiple times gets depolarized. Projecting polarized light and computing the difference of images captured with a polarization filter at two orthogonal orientations thus removes most of the multiple scattering contribution [33, 22, 25, 29]. Another method for separating direct from global reflections based on high frequency illumination patterns has recently been proposed by Nayar *et al*. [19].

Figure 1. By combining phase-shifting and polarization our method faithfully captures the 3D geometry of very translucent objects such as this alabaster Venus figurine (height $\approx$ 19cm).

In the same paper Nayar *et al*. also mention that phase-shifting [27, 36] can perform the separation and 3D scanning at the same time. For these reasons, our 3D scanning approach for translucent objects is based on phase-shifting. We demonstrate and analyze why descattering based on structured light alone is not sufficient to obtain high quality depth maps of heterogeneous translucent objects. Our proposed method therefore combines phase-shifting with polarization filtering. The increased performance is demonstrated and assessed on a variety of translucent objects.

2. Direct Reflection vs. Multiple Scattering

In this section we will discuss the relevant effects of direct reflection, multiple scattering or interreflections on projected polarized or non-polarized structured light patterns.

2.1. Direct Reflection

The light reflected at the surface towards the camera consists of different components [12, 20, 11]: direct reflection

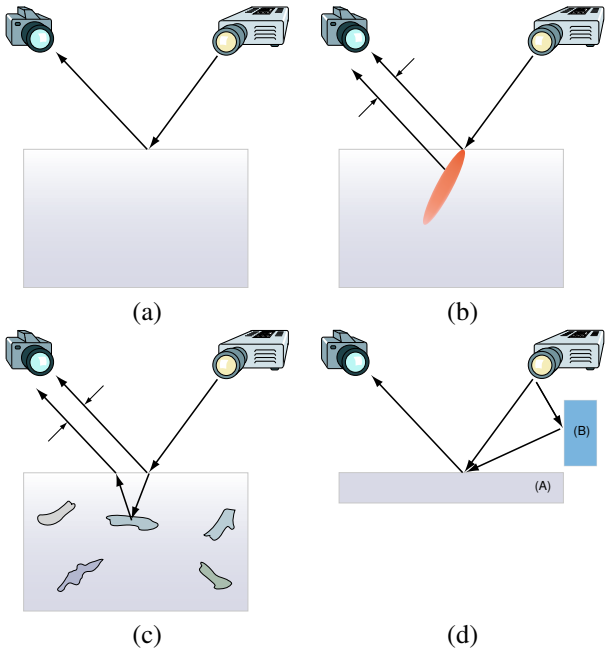

Figure 2. Rays to consider in 3D scanning. (a) 3D geometry can be estimated reliably only from the direct reflection off the surface. (b) The subsurface scattering in translucent objects can shift the observed intensity peak away from the point of incidence. (c) Opaque structures beneath the surface pollute the range estimate. (d) The signals of different projector rays are overlaid due to interreflection from another surface.

off the surface, subsurface scattering or interreflections (see Figure 2). The signal we are most interested in for 3D scanning is the directly reflected light (Figure 2a). The amount of directly reflected light depends on the surface properties such as color, roughness, *etc*. which can be summarized in the BRDF [20]. In addition, light that is reflected from a smooth surface of a dielectric (or insulating) material is partially polarized. The amount of polarization of the reflected light can be computed according to Fresnel's formulae [1] and depends on the material properties and the orientation of surface with regard to the incident and reflected ray directions. A comprehensive polarization reflectance model can be found in Wolff and Boult [34].

2.2. Multiple Scattering

The prominent effect that distinguishes translucent from opaque materials is that some light penetrates the surface and is scattered multiple times inside the object before it finally leaves the surface at some other location. Determining the 3D shape of a translucent object requires detecting the first surface intersection of the incoming light ray, *i.e*. to observe the pure direct reflection (Figure 2a). Unfortunately, the signal of the direct reflection will be rather weak since some fraction of the incident light will penetrate the surface instead of being reflected. The reflected signal will furthermore be heavily polluted by single or multiple scattering created by light incident on other scene points. As pointed out by Godin *et al*. [7] multiple scattering results in a measurable bias in the depth estimate since the location of the observed intensity peak is shifted away from the point of incidence (Figure 2b). Multiple scattering can be approximated by a diffusion process [12] and leads to a significant damping of the high frequencies in the incident illumination. Projecting shifted high frequency patterns, the global component will remain the same while changes can be observed in the direct reflection only. This can be used to remove this global effect algorithmically [19]. We will further investigate this approach in Section 4.

Multiple scattering further influences the state of polarization. While single scattering polarizes light according to the size and shape of a particle and the reference plane spanned by the direction of the incoming light and the scattered direction, multiple scattering due to the random orientation of particles to some degree depolarizes the incident light [32, 26, 25]. In Section 5 we make use of the depolarization properties to remove multiple scattering effects from the measurements.

Another important source of error is depicted in Figure 2c. Here, some structure beneath the surface actually reflects more light than the direct reflection at the surface leading to wrong depth estimates (compare Figures 6 and 4). While light reflected by those structures keeps the high frequencies of the incident light pattern we show in our experiments that it undergoes some degree of depolarization, which can be utilized.

2.3. Interreflections

Similar effects are introduced by interreflections due to nearby surfaces (Figure 2d). The signal of the direct reflection off an arbitrary surface (not necessarily translucent) is disturbed by the indirect reflection from another surface. The resulting artefacts might range from a small bias added to the depth estimate of the original surface (A) to wrongly detecting the depth of the mirror image of the other surface (B).

Depending on the reflection properties of the other surface (B) the high frequencies of the original pattern will typically be significantly reduced in the indirect reflection; for a glossy or diffuse BRDF, the illumination of a single point on surface (B) will indirectly illuminate a larger region on surface (A), hereby spreading out the signal. For second and higher order interreflections the loss of high frequencies is even more prominent.

Note, however, that interreflections might still result in linearly polarized light depending on the arrangement of surfaces (A) and (B). As a result, polarization is not always suitable for separating the direct component from interreflections.

3. Related Work

3.1. 3D Scanning

Numerous 3D scanning techniques have been developed during the last decades. A long processing pipeline is necessary to obtain a complete 3D model from a collection of range scans [14]. In this paper we concentrate just on capturing reliable range maps and do not cover further processing such as registration, merging, or smoothing. Structured light methods (see Salvi *et al*. [23] for a survey) analyze a set of images captured under well defined patterns in order to determine the correspondence between camera and projector pixels for each surface point, from which the point's depth can be computed. They range from line sweeping algorithms [4] to optimized stripe boundary codes that allow for real-time scanning [8]. Davis *et al*. [5] presented a common framework, spacetime stereo to unify stereo, structured light, and laser scanning.

While most structured light approaches simply assume to observe the undistorted measurements from direct surface reflections the phase-shifting algorithm is more robust against noise caused by global illumination effects such as subsurface scattering, as we will explain in detail in Section 4.

Other 3D geometry capturing approaches include for example photometric stereo, which Magda *et al*. [15] demonstrated for non-diffuse material. Photometric stereo is also suited to obtain the geometry of the surface's mesostructure which, considering specular reflections only, can be derived with high fidelity [3], because specular reflections are only moderately biased by low frequency global illumination effects. In [13], Kutulakos and Steger introduced a light-path triangulation theory to capture the 3D shape of refractive and specular objects. Miyazaki and Ikeuchi [16] reconstructed the surface shape of transparent objects by using polarization.

3.2. Separation of Reflection Components

This paper focuses on structured light 3D scanning of translucent objects and the most important problem here is to separate the direct reflection component from any global illumination effect. Current separation approaches are either based on polarization, which we will further discuss in Section 5, or on structured, high frequency illumination. Using images captured with a polarization filter at different orientations one can for example separate diffuse from specular reflections [18, 22, 30, 31] or attempt to remove depolarized global effects such as multiple scattering due to participating media [24, 25, 26, 29]. Making use of structured, high frequency illumination, most global effects can be removed since only direct reflection will propagate high frequencies while global effects drastically damp them [17, 19]. Wu and Tang [35] obtained a full separation into specular, diffuse, and subsurface scattering reflection components by additionally analyzing directional dependence.

4. Phase-Shifting for 3D Scanning and Reflection Separation

Nayar *et al*. [19] have developed a simple and efficient method for separating direct and global components of the light reflected by a scene. The approach is based on the insight that global effects significantly damp high frequencies (compare Section 2). Illuminating the scene with shifted high frequency patterns therefore will result in high frequencies observable in the direct reflection part only.

4.1. Descattering Properties of Phase-Shifting

Various patterns have been proposed by Nayar *et al*. [19] to perform the separation ranging from checker board and simple stripe patterns to sinusoids. As pointed out by the authors shifted sinusoids can be used simultaneously for 3D scanning since the patterns allow for deriving the phase of the sinusoid function. We implemented this technique in our 3D scanning approach as well. Assuming that the output of the projector is linear, which we establish through photometric calibration, a set of sine patterns is generated as $L_i(m,n) = 0.5\cos(\lambda m + \delta_i) + 0.5$, where λ is the frequency for all patterns and δ_i is the phase-shift for each individual pattern. Given a sufficiently high λ, the observed intensity I reflected of a scene point at camera pixel (x,y) will be

$$I_i(x,y) = \frac{1}{2}[L_d(x,y)cos(\Phi(x,y) + \delta_i) + L_d(x,y) + L_g(x,y)]. \quad (1)$$

Note that only the direct reflection L_d will depend on the phase Φ of the surface point while the global part L_g will not. The observed phase $\Phi(x,y)$ is correlated to the depth or disparity of the surface point and depends on the specific camera and projector parameters. From a set of at least three different phase shifts, *e.g.* $\delta_i \in -2\pi/3, 0, 2\pi/3$, one can separate the global and the direct components as

$$L_g = \frac{2}{3}(I_0 + I_1 + I_2) - L_d \quad \text{and} \quad (2)$$

$$L_d = \frac{2}{3}\sqrt{3(I_0 - I_2)^2 + (2I_1 - I_0 - I_2)^2}. \quad (3)$$

L_g is supposed to be in low frequency and leads to the fact that it can be cancelled out implicitly in the least square evaluation of Φ. For N evenly spaced phase shifts in one cycle the following equation computes the phase at pixel(x,y):

$$\Phi(x,y) = tan^{-1}\left(\frac{-\sum I_i \sin(\delta_i)}{\sum I_i \cos(\delta_i)}\right), \quad (4)$$

where all sums are over the N measurements, a result which has also been observed in communication theory when detecting noise corrupted signals using synchronous detection [2]. At the same time we can use the ratio γ of the observed amplitude over the observed bias as a measure for the reliability of the phase estimation:

$$\gamma = \frac{L_d}{L_d + L_g} = \frac{N\sqrt{(\sum I_i \sin(\delta_i))^2 + (\sum I_i \cos(\delta_i))^2}}{\sum I_i \sum \sin^2(\delta_i)}. \quad (5)$$

4.2. Temporal Phase-Unwrapping

Using shifted patterns with a single frequency we can detect the phase within one period of the selected frequency ($\Phi \in [0, 2\pi]$). The period however might be repeated multiple times over the entire scene. The problem is to locate the absolute unwrapped phase Ψ that uniquely identifies the pixel's phase. A number of different methods have been proposed to obtain an unwrapped phase map [6]. If the scene contains depth discontinuities the exact phase and period can be obtained by repeating the phase extraction for multiple (lower) frequencies [9, 10]. Possible approaches are choosing frequencies such that the greatest common divisor of the periods is larger than the number of columns in the projector image [28]. More robust unwrapping is obtained by creating a series of frequencies $\lambda_j = 0.5\lambda_{j-1}$ until one period spans the projector image width s resulting roughly in $F = \log_2(s)$ frequencies [10]. Given the unwrapped phase at one frequency $j+1$, the unwrapping algorithm iteratively locates the phase at step j, the next higher frequency. Starting with $j = F - 1$ and $\Psi_F = \Phi_F$ one computes the unwrapped phase at the next higher frequency by

$$\Psi_j = \Phi_j - 2\pi \text{NINT}\left(\frac{\Phi_j - 2\Psi_{j+1}}{2\pi}\right), \quad (6)$$

where NINT rounds to the nearest integer. The unwrapping itself is to some extent similar to decoding binary encoded structured light patterns [23], but more robust.

In our experiments (see Section 6) we used periods of $8, 16, 32, 64, 128, 256, 512$ and 1024 pixels. At the higher frequencies (8 and 16 pixels) we use 8 and 16 phase-shifts to obtain the best precision while the lower frequencies are only used for disambiguating the period (making rough and stable binary decisions), therefore six phase shifts turned out to be sufficient. Overall, 60 images are captured for each range scan but the number could be further reduced if necessary.

Using multiple frequencies poses the problem that Equation 1 only holds for high frequencies. For low frequencies, the global component will also vary with the phase-shift and thus the phase and depth estimates will be biased. Based on the scanning of the planar block of alabaster shown in Figure 6 we demonstrate this effect in Figure 3a by comparing

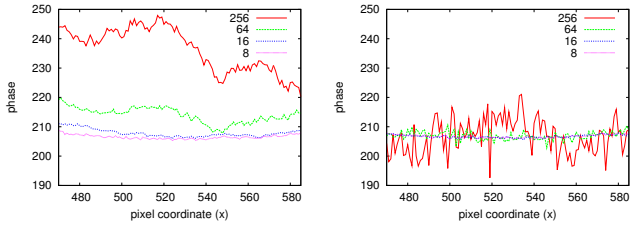

(a) (b)

Figure 3. Biased phase reconstruction for low frequency patterns. (a) Phase profiles of individual frequencies for one line on the planar alabaster block. (b) After polarization-difference imaging (Section 5) even the lower frequencies result in correct depth estimates. Notice that the curves are tilted by the same factor for illustration.

the phase estimates for different frequencies. The lower the frequency, the larger the deviation of the estimated phase for the individual frequency. A small or moderate drift at a low frequency has typically only very little effect on the combined result since the lower frequencies are just used for estimating the 2π modulo jumps. Figure 4c shows an example where the deviation on a lower frequency is larger than one period and thus introduces a major offset in the 3D scan.

In the next section we demonstrate how reliable depth profiles can be computed even for low frequencies when polarization is used in addition to phase-shifting to separate out the global component (Figure 3b and Figure 4d).

5. Polarization-Difference Imaging for Descattering

As discussed in Section 2 multiple scattering depolarizes the incoming light. Schechner *et al.* [26, 24, 25, 29] have made extensive use of this phenomena to compute clear pictures through haze or murky water by taking several polarized images from which the depolarized part can be removed afterwards. Based on the estimated signal loss induced by the participating media the authors further compute rough depth maps of the underlying scene.

In our setup depicted in Figure 5 linear polarizers are put in front of the camera and the projector. We then capture the phase-shift image sequence twice, once when the camera's polarizer axis is oriented parallel to the projector's polarizer axis, yielding $I_j^{\parallel}$, and a second time using cross-polarization, $I_j^{\perp}$. A polarization difference image [22, 30] is then computed as

$$I_j^{\Delta} = |I_j^{\parallel} - I_j^{\perp}|. \quad (7)$$

The idea is that depolarized light will add exactly the same contribution to both image sequences, independent of the camera's filter orientation, and thus will be completely removed in I_j^{Δ}. Based on I_j^{Δ} we then perform the 3D reconstruction.

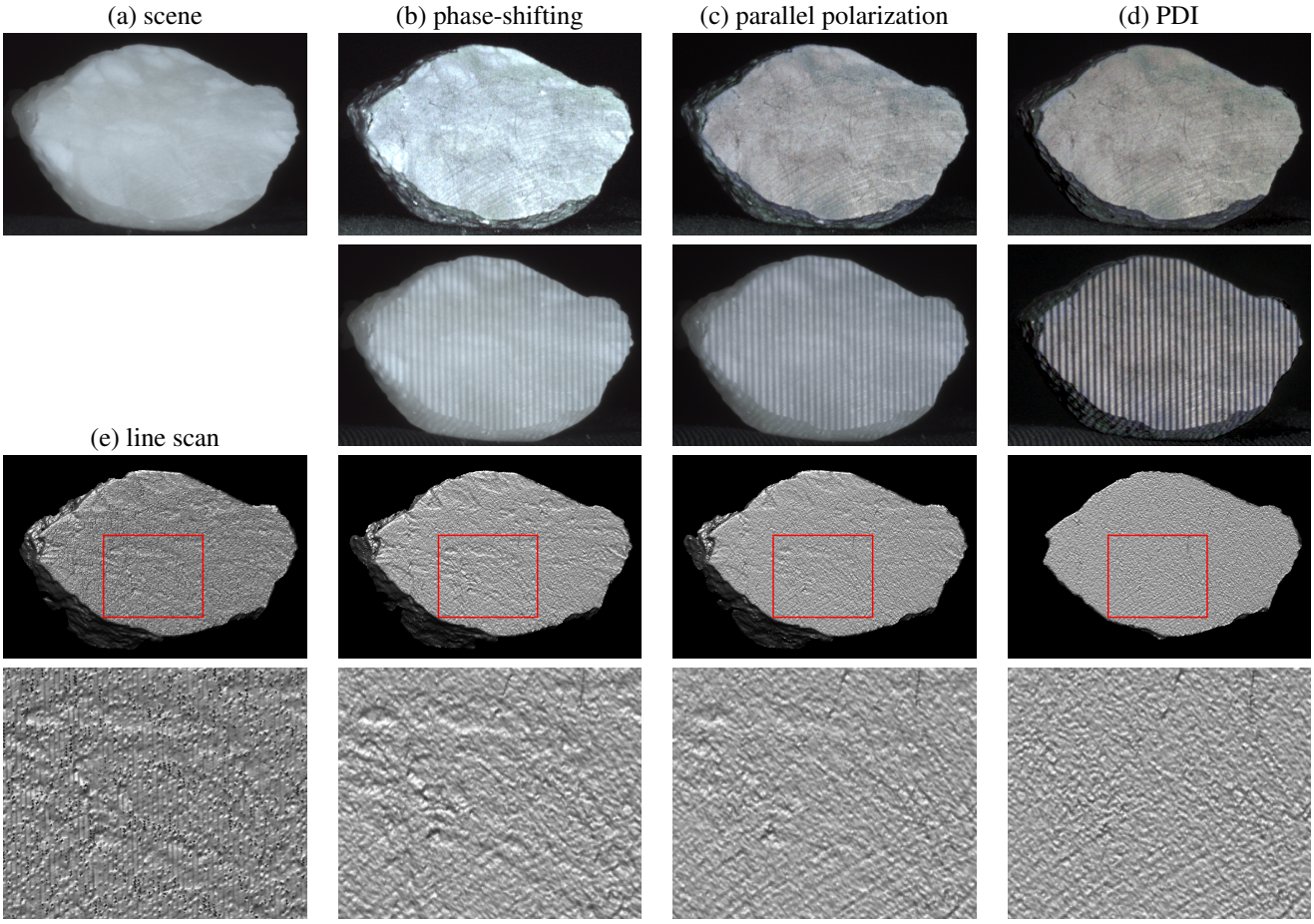

Figure 6. Reconstruction results for a planar surface of heterogeneous alabaster. First row: (a) Photograph. While the direct component L_d (b) extracted using no polarization filters clearly contains some subsurface structures they are partially removed by parallel polarization $L_d^{\parallel}$ (c) and not present after applying PDI L_d^{Δ} (d). Second row: The contrast in the high frequency input images is improved by parallel polarization and further by PDI. Third and fourth row (magnified region): Geometry reconstruction results for (e) line sweeping, (b) phase-shifting without polarization, (c) with parallel polarization, and (d) with PDI. The influence of the subsurface structures on the final 3D geometry has been completely removed by PDI.

Figure 6 demonstrates the effect of polarization filtering on the quality of the 3D reconstruction of a quite planar block of alabaster. The most important difference between 3D reconstruction by phase-shifting without polarization filtering and with polarization-difference imaging applied is that scattering events beneath the surface are much better removed in the latter case. Using PDI, the contrast and thus the signal of the input images is largely improved (bottom row of Figure 6). However, as will be discussed in the result section, there are some scenes where the PDI approach filters out too much of the direct reflection. In these cases using the image sequence with parallel orientation of the polarization filters provides a good trade-off between no polarization and PDI.

6. Results

In the following section we assess the descattering capabilities of phase-shifting with and without polarization on a set of translucent scenes: a highly translucent, almost homogeneous alabaster figurine (Figure 1 and 7), a filled, translucent vase (Figure 4), a heterogeneous planar slab of alabaster (Figure 6), some grapes and a starfruit (Figure 7). Except for removing spurious background pixels and pixels having a too weak signal no further processing, *i.e.* noise removal or smoothing has been applied to the results in this paper.

6.1. Setup

All images in this paper have been acquired with a 14-bit 1360×1024-pixel Jenoptik ProgRes CFcool CCD camera and a Mitsubishi XD490U XGA DLP Projector whose native resolution is 1024×768. We performed a photometric

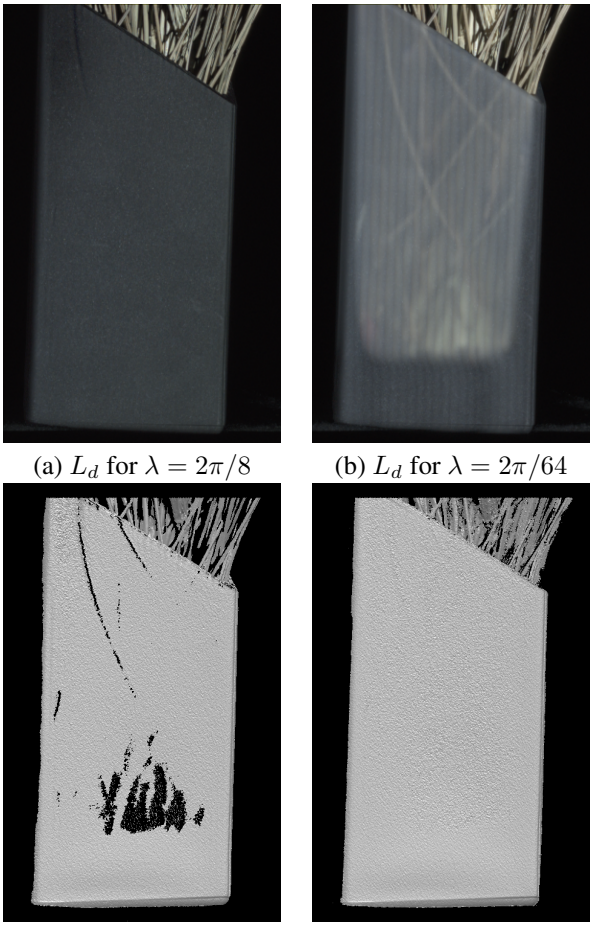

(a) L_d for $\lambda = 2\pi/8$ (b) L_d for $\lambda = 2\pi/64$

(c) phase-shifting (d) PDI

Figure 4. For this translucent vase filled with lavender, the reconstructed direct reflection is dependent on the frequency of the illumination pattern. (a) Most subsurface scattering is removed using the highest frequency. (b) At lower frequencies structures beneath the surface contribute to the direct component polluting the phase-unwrapping results in (c). (d) Using PDI the influence of subsurface structures is largely reduced and the desired shape is captured.

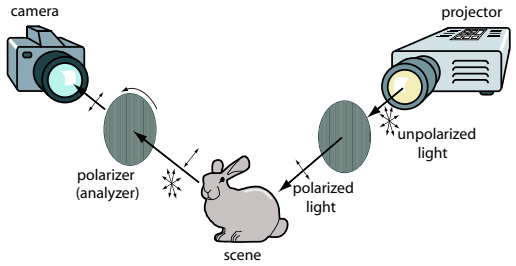

Figure 5. Our setup for polarization-difference imaging (PDI). The projector is equipped with a linear polarization filter at fixed orientation. The camera captures two image sequences with parallel and with perpendicular orientation of the polarization filters.

calibration for both devices and captured HDR images [21] using four different exposures. The measured maximum simultaneous contrast of a sine pattern with a period of 8 pixels reflected by a gray card is 180:1 (max/min). We performed geometric calibration between the camera and the projector [37]. Linear polarization filters have been placed in front of the projector and the camera to acquire the PDI image sequences.

6.2. Structured Light Results

Descattering based on phase-shifting without polarization can deal pretty well with translucent objects and clearly removes some amount of the subsurface scattering (Figure 7), as predicted by Nayar *et al*. [19]. The phase-unwrapping, however, relies on low frequency patterns which clearly suffer from global effects (see Section 5). Furthermore, structures beneath but close to the surface will have some influence on the estimated direct component which is unwanted in the context of 3D scanning (Figure 4 and 6).

Sweeping a single line is an alternative to phase-shifting and performs surprisingly similar. As can be seen in Figure 6 even for highly translucent objects one obtains a reasonable 3D scan if high quality equipment and HDR sequences are used. The noise in the figure indicates that the SNR of line sweeping compared to phase-shifting is considerably lower. Although line sweeping is still sensitive to the bias introduced by subsurface scattering or subsurface structures (Section 2) global effects are minimized by the comparably small amount of incident light concentrated on a small region.

6.3. Polarization Results

Polarization-difference imaging also separates the direct from the global component very well. It faithfully removes all traces of subsurface structures. At grazing angles PDI however filters out too much of the direct reflection (see Figure 7). It is worthwhile to note that depending on the surface properties also some fraction of the direct reflection might be depolarized. This fraction will also be removed in the polarization difference image. For some scenes, we actually observed a better contrast of direct vs. global reflection in the parallel polarization setting $I_j^{\parallel}$ producing smoother 3D scans (see Figures 7, bottom row). Even though parallel polarization in theory only removes some fraction of multiple scattering effects (compare second row in Figure 6), combining it with phase-shifting adds the descattering capabilities of both techniques. Figure 6 further shows that parallel polarization also renders phase-shifting slightly more robust against subsurface structures, though not as robust as PDI. On the other hand parallel polarization is much easier to acquire since it requires only half the amount of images and a fixed orientation of the filters.

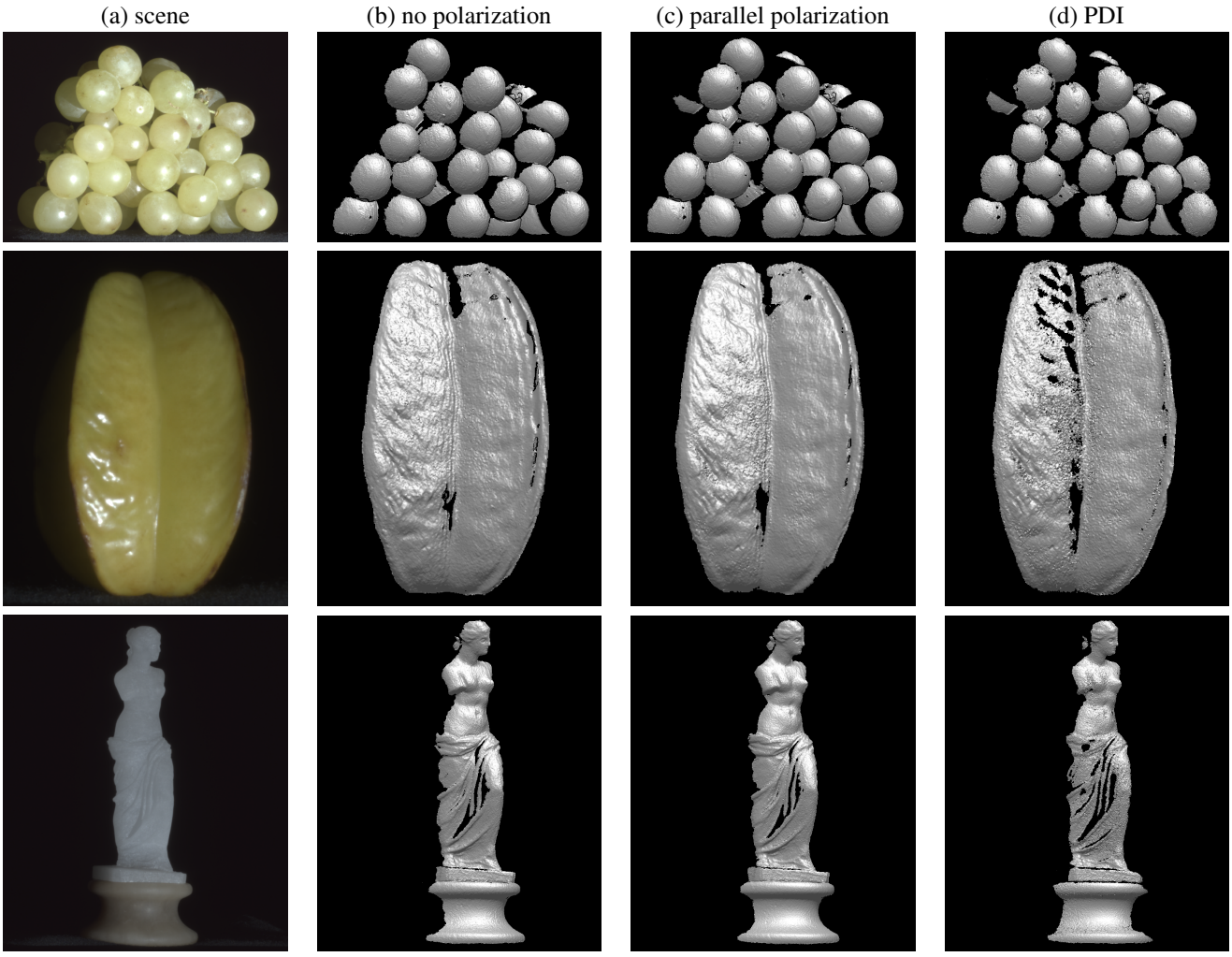

Figure 7. Reconstruction results for a selection of translucent objects. For these scenes the reconstruction results of phase-shifting without polarization (b) and with parallel polarization (c) are of comparable quality since the objects are mostly homogeneous. At grazing angles too much signal from the direct reflection is filtered out by PDI (d) resulting in more holes and noisier depth maps.

7. Conclusion

By combining phase-shifting with polarization filtering we introduced a robust 3D scanning technique for translucent objects. A careful analysis of phase-shifting without polarization, combined with parallel polarization and with polarization-difference imaging has shown that some of the shortcomings of pure phase-shifting such as its sensitivity to subsurface structures can be overcome. Even though PDI has the ability to robustly remove all global effects due to subsurface scattering which otherwise renders accurate 3D scanning a hard problem, parallel polarization sometimes provides a better SNR resulting in less noisy range maps. Depending on the richness of subsurface structure, the planarity of the object and the sensitivity of the camera one might choose one method over the other.

The descattering property of polarization can also be used by other structured light techniques, such as gray code, binary code, De Bruijn sequences *etc*. [23]. It would be also interesting to exploit the hybrid method that can intelligently choose the right method to do reliable 3D scanning for general translucent objects. We expect there will be some further descattering based methods that can help accurate and robust 3D reconstruction of translucent objects or even general scenes including a wide range of materials.

Acknowledgements

We would like to thank the anonymous reviewers for their insightful comments. Thanks to Michael Goesele for his valuable advice. Thanks to Michael Heinz for his help in doing experiments. We are grateful to Yan Wang for her assistance in the project. This work has been partially funded by the Max Planck Center for Visual Computing and Communication (BMBF-FKZ01IMC01).

References

[1] M. Born, E. Wolf, and A. B. Bhatia. *Principles of Optics*. Cambridge University Press, 1999.

[2] J. H. Bruning, D. R. Herriott, J. E. Gallagher, D. P. Rosenfeld, A. D. White, and D. J. Brangaccio. Digital wavefront measuring interferometer for testing optical surfaces and lenses. *Appl. Opt.*, 13:2693–2703, 1974.

[3] T. Chen, M. Goesele, and H.-P. Seidel. Mesostructure from specularity. In *Proceedings of CVPR*, pages 1825–1832, 2006.

[4] B. Curless and M. Levoy. Better optical triangulation through spacetime analysis. In *Proceedings of ICCV*, pages 987–994, 1995.

[5] J. Davis, D. Nehab, R. Ramamoorthi, and S. Rusinkiewicz. Spacetime stereo: a unifying framework for depth from triangulation. *PAMI*, 27(2):296–302, 2005.

[6] D. C. Ghiglia and M. D. Pritt. *Two-dimensional phase unwrapping: theory, algorithms, and software*. Wiley, New York, 1998.

[7] G. Godin, J.-A. Beraldin, M. Rioux, M. Levoy, L. Cournoyer, and F. Blais. An assessment of laser range measurement of marble surfaces. In *Proceedings of Fifth Conference on optical 3-D measurement techniques*, pages 49–56, 2001.

[8] O. Hall-Holt and S. Rusinkiewicz. Stripe boundary codes for real-time structured-light range scanning of moving objects. In *Proceedings of ICCV*, pages 359–366, 2001.

[9] J. M. Huntley and H. O. Saldner. Temporal phase unwrapping algorithm for automated interferogram analysis. *Appl. Opt.*, 32:3047–3052, 1993.

[10] J. M. Huntley and H. O. Saldner. Phase unwrapping: application to surface profiling of discontinuous objects. *Appl. Opt.*, 36:2770–2775, 1997.

[11] A. Ishimaru. *Wave Propagation and Scattering in Random Media*. Academic Press, 1978.

[12] H. W. Jensen, S. R. Marschner, M. Levoy, and P. Hanrahan. A Practical Model for Subsurface Light Transport. In *SIGGRAPH 2001*, pages 511–518, 2001.

[13] K. N. Kutulakos and E. Steger. A theory of refractive and specular 3D shape by light-path triangulation. In *Proceedings of ICCV*, pages 1448–1455, 2005.

[14] M. Levoy, K. Pulli, B. Curless, S. Rusinkiewicz, D. Koller, L. Pereira, M. Ginzton, S. Anderson, J. Davis, J. Ginsberg, J. Shade, and D. Fulk. The digital michelangelo project: 3D scanning of large statues. In *SIGGRAPH*, pages 131–144, 2000.

[15] S. Magda and T. Zickler. Beyond Lambert: reconstructing surfaces with arbitrary BRDFs. In *Proceedings of ICCV*, pages 391–398, 2001.

[16] D. Miyazaki and K. Ikeuchi. Inverse polarization raytracing: estimating surface shape of transparent objects. In *Proceedings of CVPR*, pages 910–917, 2005.

[17] S. Narasimhan, S. Nayar, B. Sun, and S. Koppal. Structured light in scattering media. *Proceedings of ICCV*, pages 420–427, 2005.

[18] S. K. Nayar, X. S. Fang, and T. Boult. Separation of reflection components using color and polarization. *IJCV*, 21(3):163–186, 1997.

[19] S. K. Nayar, G. Krishnan, M. D. Grossberg, and R. Raskar. Fast separation of direct and global components of a scene using high frequency illumination. *ACM Transactions on Graphics*, 25(3):935–944, 2006.

[20] F. E. Nicodemus, J. C. Richmond, J. J. Hsia, I. W. Ginsberg, and T. Limperis. Geometrical considerations and nomenclature for reflectance. National Bureau of Standards, 1977.

[21] M. A. Robertson, S. Borman, and R. L. Stevenson. Estimation-theoretic approach to dynamic range enhancement using multiple exposures. *J. Electronic Imaging*, 12(2):219–285, 2003.

[22] M. P. Rowe and J. E. N. Pugh. Polarization-difference imaging: a biologically inspired technique for observation through scattering media. *Optics Letters*, 20(6):608–610, 1995.

[23] J. Salvi, J. Pages, and J. Batlle. Pattern codification strategies in structured light systems. *Pattern Recognition*, 37(4):827–849, 2004.

[24] Y. Y. Schechner and N. Karpel. Clear under water vision. In *Proceeding of CVPR*, pages 536–543, 2004.

[25] Y. Y. Schechner and N. Karpel. Recovery of underwater visibility and structure by polarization analysis. *IEEE Journal of Oceanic Engineering*, 30(3):570–587, 2005.

[26] Y. Y. Schechner, S. G. Narsimhan, and S. K. Nayar. Polarization-based vision through haze. *Applied Optics*, 42(3):511–525, 2003.

[27] V. Srinivasan, H.-C. Liu, and M. Halioua. Automated phase-measuring profilometry: A phase mapping approach. *Appl. Opt.*, 24:185–188, 1985.

[28] M. Tarini, H. P. A. Lensch, M. Goesele, and H.-P. Seidel. 3d acquisition of mirroring objects. *Graphical Models*, 67(4):233–259, July 2005.

[29] T. Treibitz and Y. Y. Schechner. Instant 3descatter. In *Proceedings of CVPR*, pages 1861–1868, 2006.

[30] J. S. Tyo, M. P. Rowe, E. N. Pugh, and N. Engheta. Target detection in optically scattering media by polarization difference imaging. *App. Opt.*, 35:639–647, 1996.

[31] S. Umeyama and G. Godin. Separation of diffuse and specular components of surface reflection by use of polarization and statistical analysis of images. *PAMI*, 26(5):639–647, 2004.

[32] H. C. van de Hulst. *Light scattering by small particles*. Courier Dover Publications, New York, Dover, 1981.

[33] L. B. Wolff. Polarization camera for computer vision with a beam splitter. *Journal of the Optical Society of America*, 11:2935–2945, 1994.

[34] L. B. Wolff and T. E.Boult. Constraining object features using a polarization reflectance model. *PAMI*, 13(7):635–657, 1991.

[35] T.-P. Wu and C.-K. Tang. Separating specular, diffuse, and subsurface scattering reflectances from photometric images. In *Proceedings of ECCV*, pages 419–433, 2004.

[36] S. Zhang and S.-T. Yau. High-resolution, real-time absolute 3-D coordinate measurement based on the phase shifting method. *Opt. Express*, 14:2644–2649, 2006.

[37] Z. Zhang. A flexible new technique for camera calibration. *PAMI*, 22(11):1330–1334, 2000.